Working Example: Comparing Global Predictions of Dynamic Topography or the Geoid With Observations

Gareth G. Roberts & Conor O'Malley
gareth.roberts@imperial.ac.uk

1 Introduction

This document describes a minimum working example to generate statistics used to assess similarities and dissimilarities of dynamic topographies and geoids from different global grids. It assumes that we are comparing 'observed' dynamic topography, generated using residual ocean age-depth measurements [Hoggard et al., 2016a, Holdt et al., 2022], or the observed geoid [EIGEN5c Foerste et al., 2008], with predictions from global mantle convection simulations [e.g. TERRA; Davies et al., 2025]. The following is largely adapted from O'Malley et al. [2024].

To aid comparison at specific scales, first the two global grids are expanded into spherical harmonic form. Any real, square-integrable function over the surface of the Earth can be described as a function of longitude θ and latitude ϕ by a linear combination of spherical harmonics of degree l and order m,

$$f(\theta,\phi) = \sum_{l=1}^{L} \sum_{m=-l}^{l} f_{lm} Y_{lm}(\theta,\phi), \tag{1}$$

where the spherical harmonic functions Y_{lm} are the natural orthogonal set of basis functions on the sphere, and f_{lm} are the spherical harmonic coefficients [see e.g. Forte, 2007, Wieczorek and Meschede, 2018, for discussion of spherical harmonics and application to geophysical problems]. The spherical harmonic coefficients, f_{lm}, for irregularly sampled surfaces (e.g. dynamic topography) can be calculated using a least-squares methodology [see e.g. Hoggard et al., 2016a, Wieczorek and Meschede, 2018]. For regularly sampled grids, the expansion can be achieved by by performing Fast Fourier Transforms in longitude and integrating over latitude, see e.g. the pyshtools `expand` modules from [Wieczorek and Meschede, 2018]. The power at each degree, l, is given by

$$P_l = \sum_{m=-l}^{l} f_{lm}^2. \tag{2}$$

Several different normalizations are commonly used in the geodynamic community, which can make the comparisons of spherical harmonic coefficients (and derived quantities, e.g. power) less straightforward than might be first thought. Wieczorek and Meschede [2018] provide a helpful overview of many of the 'standard' normalizations used. It is obviously important to ensure the same normalizations are used to generate the grids being compared. Often this requires conversion and consideration of whether the Condon-Shortly phase factor of $(-1)^m$ is included or not. The following statistics are calculated to aid comparison.

1.1 Euclidean Comparisons of Amplitudes

First, we calculate root-mean-squared difference, χ, between predicted surface deflections in the spatial domain,

$$\chi = \sqrt{\frac{1}{N}\sum_{n=1}^{N} w_\phi \left(h_n^a - h_n^b\right)^2}, \tag{3}$$

where h_n^a and h_n^b are predicted surface deflections from the two models being compared. N = number of points in the $1 \times 1^\circ$ gridded maps being compared. The prefactor w_ϕ is proportional to $\cos\phi$, where ϕ is latitude, and is included to correct biases in cell size with latitude; mean $w_\phi = 1$. This metric is closely associated with the mean vertical distance (L^2-norm distance) between predicted and reference surfaces, i.e., $\Delta\bar{h} = 1/N \sum_{n=1}^{N} w_\phi |h_n^a - h_n^b|$. These metrics are sensitive to differences in amplitudes and locations of surface deflections.

1.2 Spectral Correlation Coefficients

Secondly, to aid comparisons of surface deflections as a function of scale they are converted into the frequency domain using spherical harmonics. The degree-correlation spectrum, r_l, is calculated using pyshtools [Wieczorek and Meschede, 2018], such that

$$r_l = \frac{Sf_1f_2}{\sqrt{Sf_1f_1 \cdot Sf_2f_2}} \tag{4}$$

where f_1 and f_2 are the spherical harmonic coefficients of the two estimates of surface deflection being compared. They vary as a function of order, m, and degree, l; $f = f_l^m$. Sf_af_b is the cross spectrum of the two functions f_a and f_b. We note that $-1 \leq r_l \leq 1$, and we calculate the mean value, $\overline{r_l} = 1/L \sum_{l=1}^{L} r_l$, where L is total number of degrees. Thirdly, the correlation of the entirety of both functions can be estimated following Forte et al. [2015], such that

$$r = \frac{\sum f_1^* f_2}{\sqrt{\sum f_1^* f_1}\sqrt{\sum f_2^* f_2}}, \quad \text{where} \quad \sum = \sum_{m=-l}^{+l}, \tag{5}$$

where $*$ indicates complex conjugation [see also Becker and Boschi, 2002, O'Connell, 1971]. This metric is not sensitive to the amplitudes of surface deflections.

1.3 Comparing Calculated Power Spectra

Finally, differences in power spectra between between predicted and independent surface deflections are calculated such that

$$\chi_p = \sqrt{\frac{1}{L}\sum_{l=1}^{L}\left(\log_{10}P_l - \log_{10}P_l^K\right)^2} + \sqrt{\frac{1}{L}\sum_{l=1}^{L}\left(\log_{10}P_l - \log_{10}P_l^H\right)^2}, \tag{6}$$

where L is the number of spherical harmonic degrees being considered. P_l^K and P_l^H are total power per degree estimated independently from Kaula's law or residual oceanic age-depth measurements, respectively [Equation 7; Hoggard et al., 2016b, Holdt et al., 2022]. Once power spectra are calculated it is straightforward to compare their spectral slopes, which can be used to assess whether broad patterns of surface deflections are similar even if their amplitudes do not match.

Using the total power per degree convention, Hoggard et al. [2016a] derived a rule-of-thumb for estimating the power spectrum of dynamic topography (see their Supporting Information), P_l^K, using Kaula [1963]'s approximation for the long-wavelength gravity field of Earth as a function of l:

$$P_l^K \approx \left(\frac{GM}{ZR^2}\right)^2 \left(\frac{2}{l} - \frac{3}{l^2} + \frac{1}{l^4}\right), \tag{7}$$

where G is the gravitational constant, $M = 5.97 \times 10^{24}$ kg is the mass of the Earth, $R \approx 6370$ km is Earth's radius. The value of admittance, Z, between gravity and topography varies as a function of viscosity, as well as the depth and wavelength of internal density anomalies because of the depth- and degree-dependence of their respective sensitivity kernels [see e.g. Colli et al., 2016, and references therein]. However, in the upper mantle, which contributes most to surface deflections, the topography and gravity kernels are approximately proportional to one another across all but the lowest spherical harmonic degrees, even when this layer is assumed to be of relatively low viscosity [see e.g. Colli et al., 2016, their Figure 2]. This behavior can explain why Hoggard et al. [2016a] found that assuming an average value of $Z = 12$ mGal km^{-1} provides a reasonable approximation of observed residual topographic trends, thus we make use of that value. Finally, it is useful to note that Jeans [1923] related spherical harmonic degree to wavelength λ, which at Earth's surface can be approximated via $\lambda \approx 2\pi R/\sqrt{l(l+1)}$.

2 Implementation

The associated density files produced from the TERRA runs are usually have the prefix `density_sph.037`, where the highest number (e.g. 37) indicates the output from the final time step, i.e. 0 Ma. The associated radial viscosity file must also be downloaded. If the TERRA model has non-radial viscosities they must first be converted into a reasonable one-dimensional function (e.g. from the radial averages). Once these two files are available the following `bash` script can be executed

```
> ./run.sh
```

which inserts the spherical harmonic density and radial viscosity files and into `./GEOID`, which is generated following the instructions at `https://doi.org/10.5281/zenodo.12696774`. Note that the executable `GEOID` is generated and executed when `run.sh` is run.

`run.sh` assumes that a file listing the values of constants, `const.dat`, exists. That file is expected to contain the values of constants used to produce the TERRA run. They are, ordered by column number:

1. `Output name`: Name of output directory to store results created during this analyses.
2. `Density`: Location and name of density file (using ending `*density_sph.0*`).
3. `Visc`: Location and name of the radial viscosity file.
4. `Max degree (DT calc)`: Maximum spherical harmonic degree, L, to perform model comparisons, usually 50.
5. `Min depth (for DT calc. km)`: Cut-off depth for dynamic topography calculation, densities above this value are excluded from the calculation (usually set to 0, i.e. to include all values up to the surface of the model).
6. `Kappa (1=compressible, else incompressible)`: Confirm whether TERRA model was compressible or not.
7. `rho_w`: Density of overlying fluid, usually assumed to be water, with density $\rho_w = 1.05 \times 10^3$ kg/m^3.
8. `visc_0`: Reference viscosity, $\eta_\circ$, with value determined by what is used in the TERRA run, usually $\eta_\circ = 10^{21}$ Pa s.

9. `l_min`: Minimum degree, l, used to perform model comparisons, usually 1.
10. `bgrho`: Background density, now usually a redundant parameter.
11. `grav10`: 1 = assume gravity is constant value ($g = 10$ m /s^2), 0 = self-gravitation.
12. `bdry (surface: 1 = free, 0 = no-slip)`: Surface boundary condition, i.e. free- or no-slip.
13. `bdry_bot (CMB: 1 = free, 0 = no-slip)`: Core-mantle boundary condition (free- or no-slip).

Output to the terminal from running `run.sh`, for the single model in the provided working example, should include the following statistics, which are produced by the `GEOID` code:

```
running GEOID...
-------------------------------------
 Processor reporting: 0
-------------------------------------
  Geoid Correlation:
                                0.268
  Free-Air Gravity Correlation:
                               -0.114
  Dynamic Topography Correlation:
                                0.174
  CMB     Topography Correlation:
                                0.279
  Max Geoid:
                              517.190
  Max SurfTopography:
                            21571.665
-------------------------------------
  Elapsed Time:             00:00':04"
done running GEOID.
```

Dynamic topography and the geoid (predictions and reference values) and associate statistics can be plotting by running the `bash script`:

```
> plot_mc2_paper_fulltopo_geoidstats.gmt.
```

That and all following plotting scripts work with GMT [v6.4; Wessel et al., 2019]. Various additional (`bash` and `python` v3.x) scripts that support the plotting are included in the minimum working directory provided, e.g. `my_histo_global_sph_adj.py`, `spectrum.py`, `write_constants_h.sh`, `cross_spectrum.py`, `forte_calc_corr_ggr.py`, some require `pyshtools` to be installed (see `https://shtools.github.io/SHTOOLS/python-instal`
This particular plotting script will calculate the statistics again (producing values that should be identical to those produced by `calc_stats_all_mc2_geoid_dt.sh`; see below). It should produce a figure that looks like the following one. The script `cleanup.sh` can be executed to clean up the directory if you wish.

Finally, a benchmark can be produced by running:

```
> plot_like_for_like_paper_fulltopo_geoidstats.gmt
```

which is a simple modification of `plot_mc2_paper_fulltopo_geoidstats.gmt`, calculating and plotting the statistics for reference vs. reference models, as a check that the way statistics are calculated is sensible.

Once `GEOID` has been run for each model, statistics for those (singular or many) model comparisons can be produced by running the following script, which also writes the statistics to output files (separate files

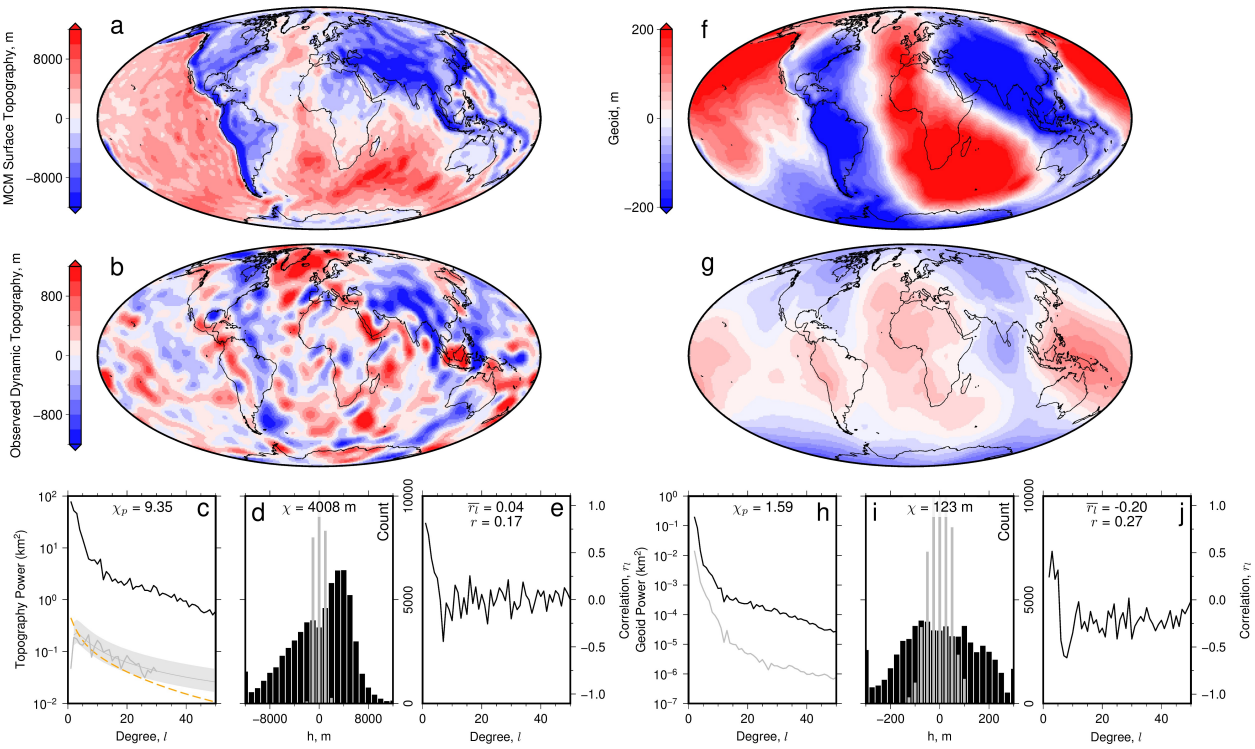

Figure 1: Example output from running `> plot_mc2_paper_fulltopo_geoidstats.gmt`. Comparison of modern surface deflections and the geoid predicted by mantle convection model (MCM; `mc2_m_cc_066_u`) with independent observations up to $l = 50$ (see body text for details). (a) Water-loaded surface deflections predicted by MCM. (b) Calculated residual topography from Hoggard et al. [2016b]. (c) Solid black = power spectrum of topography shown in panel a. Thin grey curve and band = expected dynamic topography from Kaula's rule using admittance $Z = 12 \pm 3$ mGal km^{-1}. Thick grey = power spectra of residual topography shown in panel b. Orange dashed = expected power spectra for water-loaded residual topography from Holdt et al. [2022]. (d) Black/grey = histograms of amplitudes shown in panels a/b. (e) Spectral correlation coefficients, r_l, for panels a and b. (f) Black = power spectrum of geoid calculated using TERRA. Grey = Eigen5c Foerste et al. [2008]. (g) Black/grey = histograms of geoid amplitudes in MCM/Eigen5c models. (h) Correlation coefficients for MCM/Eigen5c. Note annotated values of χ_p, χ, $\overline{r_l}$ and r are discussed in the body text.

for dynamic topography and the geoid):

`> calc_stats_all_mc2_geoid_dt.sh`.

Example output from that script, stored in `dt_scores_mc2_4dp.dat` is

```
MODEL CHI_P CHI OVERLINE_RL R MC2NAME
147 9.3522 4008 0.0421 0.1735 ./INPUT/DENSITY_INPUTS/m_cc_066_u
```

where the column names refer to the model number (see `const.dat`) and the statistics calculated in Sections 1.1–1.3: `CHI_P` = χ_p, `CHI` = χ, `OVERLINE_RL` = $\overline{r_l}$, `R` = r. `MC2NAME` stores the name of the model run archived in the TERRA simulation log (called e.g. `*MC2_Simulation_Log*`).

Acknowledgments

TERRA simulations and spherical harmonic representations of model predictions were produced by J. Panton, A. Plimmer and J. H. Davies. We thank S. Ghelichkhan for his help and for making the code archived at `https://doi.org/10.5281/zenodo.12696774` available to us. We also thank F. Richards and V. Fernandes for their help.

References

M. J. Hoggard, N. White, and D. Al-Attar. Global dynamic topography observations reveal limited influence of large-scale mantle flow. *Nature Geoscience*, 9(May):1–8, 2016a. ISSN 1752-0894. doi: 10.1038/ngeo2709.

M. C. Holdt, N. J. White, S. N. Stephenson, and B. W. Conway-Jones. Densely Sampled Global Dynamic Topographic Observations and Their Significance. *Journal of Geophysical Research: Solid Earth*, 127: 1–32, 2022.

C Foerste, F Flechtner, R Schmidt, R Stubenvoll, M Rothacher, J Kusche, K.-H. Neumayer, R Biancale, J.-M. Lemoine, F Barthelmes, J Bruinsma, R Koenig, and U Meyer. EIGEN-GL05C - A new global combined high-resolution GRACE-based gravity field model of the GFZ-GRGS cooperation. *Geophysical Research Abstracts*, 10(April 2006):Abstract No. EGU2008–A–06944, 2008.

J. H. Davies, J. Panton, I. Altoe, M. Andersen, P. Béguelin, A. Biggin, C. Davies, T. Elliott, Y. A. Engbers, V. M. Fernandes, A. M. G. Ferreira, S. Fowler, S. Ghelichkhan, B. J. Heinen, P. Koelemeijer, F. Latallerie, W. Li, G. Morgan, S. J. Mason, R. Myhill, A. Nowacki, C. P. O'Malley, A. Plimmer, D. Porcelli, N. Récalde, G. G. Roberts, J. B. Rodney, J. Shea, O. Shorttle, W. Sturgeon, A. M. Walker, J. Ward, and J. Wookey. How to assess similarities and differences between mantle circulation models and earth using disparate independent observations. *Proceedings of the Royal Society A: Mathematical, Physical and Engineering Sciences*, 481(2315):20240827, 2025. doi: 10.1098/rspa.2024.0827. URL `https://royalsocietypublishing.org/doi/abs/10.1098/rspa.2024.0827`.

C. P. B. O'Malley, G. G. Roberts, J. Panton, F. D. Richards, J. H. Davies, V. M. Fernandes, and S. Ghelichkhan. Reconciling surface deflections from simulations of global mantle convection. *Geoscientific Model Development*, 17(24):9023–9049, 2024. doi: 10.5194/gmd-17-9023-2024. URL `https://gmd.copernicus.org/articles/17/9023/2024/`.

A. M. Forte. Constraints on Seismic Models from Other Disciplines - Implications for Mantle Dynamics and Composition. In Barbara Romanowicz and Adam Dziewonski, editors, *Seismology and the Structure of the Earth*, chapter 1.23, pages 805–858. Elsevier B.V., 2007. ISBN 9780444527486. doi: 10.1016/B978-044452748-6.00027-4.

Mark A. Wieczorek and Matthias Meschede. SHTools: Tools for Working with Spherical Harmonics. *Geochemistry, Geophysics, Geosystems*, 19:1–19, 2018. doi: 10.1029/2018GC007529.

A. M. Forte, N. A. Simmons, and S. P. Grand. Constraints on Seismic Models from Other Disciplines - Constraints on 3-D Seismic Models from Global Geodynamic Observables: Implications for the Global Mantle Convective Flow. In *Treatise on Geophysics: Second Edition*, volume 1, pages 853–907. Elsevier, 2015. ISBN 9780444538031. doi: 10.1016/B978-0-444-53802-4.00028-2.

Thorsten W. Becker and Lapo Boschi. A comparison of tomographic and geodynamic mantle models. *Geochemistry, Geophysics, Geosystems*, 3(1):1–48, 2002. ISSN 15252027. doi: 10.1029/2001GC000168.

Richard J. O'Connell. Pleistocene Glaciation and the Viscosity of the Lower Mantle. *Geophysical Journal of the Royal Astronomical Society*, 23(3):299–327, 1971. ISSN 1365246X. doi: 10.1111/j.1365-246X.1971.tb01823.x.

M. J. Hoggard, N. White, and D. Al-Attar. Supplementary Information for "Global dynamic topography observations reveal limited influence of large-scale mantle flow". *Nature Geoscience*, 9(6):1–34, 2016b. ISSN 17520908. doi: 10.1038/ngeo2709.

William M. Kaula. Determination of the Earth's Gravitational Field. *Reviews of Geophysics*, 1(4):507–551, 1963.

L. Colli, S. Ghelichkhan, and H.-P. Bunge. On the ratio of dynamic topography and gravity anomalies in a dynamic Earth. *Geophysical Research Letters*, 43:2510–2516, 2016. ISSN 19448007. doi: 10.1002/2016GL067929.

J. H. Jeans. The Propagation of Earthquake Waves. *Proceedings of the Royal Society of London A*, 102 (718):554–574, 1923.

P. Wessel, J. Luis, L. Uieda, R. Scharroo, F. Wobbe, W. H. F. Smith, and D. Tian. The Generic Mapping Tools Version 6. *Geochemistry, Geophysics, Geosystems*, 20:1–9, 2019. ISSN 1525-2027. doi: 10.1029/2019gc008515.